JGR Earth Surface

RESEARCH ARTICLE
10.1029/2023JF007453

Rock Glacier Movement and Debris Transport Over Annual to Multi-Millennial Timescales

Jeffrey S. Munroe[1], Benjamin J. C. Laabs[2], Lee B. Corbett[3], Paul R. Bierman[3], and Alexander L. Handwerger[4,5]

[1]Department of Earth & Climate Sciences, Middlebury College, Middlebury, VT, USA, [2]Department of Earth, Environmental, and Geospatial Sciences, North Dakota State University, Fargo, ND, USA, [3]Rubenstein School for Environment and Natural Resources, University of Vermont, Burlington, VT, USA, [4]Joint Institute for Regional Earth System Science and Engineering, University of California, Los Angeles, Los Angeles, CA, USA, [5]Jet Propulsion Laboratory, California Institute of Technology, Pasadena, CA, USA

Key Points:

- We investigated an active rock glacier currently moving at ~10 cm yr^{-1}
- The rock glacier formed at the start of the Holocene (~10 ka)
- The rock glacier exhibited a long-term average flow rate of ~3 cm yr^{-1}

Supporting Information:

Supporting Information may be found in the online version of this article.

Correspondence to:

J. S. Munroe,
jmunroe@middlebury.edu

Citation:

Munroe, J. S., Laabs, B. J. C., Corbett, L. B., Bierman, P. R., & Handwerger, A. L. (2024). Rock glacier movement and debris transport over annual to multi-millennial timescales. *Journal of Geophysical Research: Earth Surface*, *129*, e2023JF007453. https://doi.org/10.1029/2023JF007453

Received 22 SEP 2023
Accepted 21 MAR 2024

Author Contributions:

Conceptualization: Jeffrey S. Munroe
Data curation: Jeffrey S. Munroe
Formal analysis: Jeffrey S. Munroe, Benjamin J. C. Laabs, Alexander L. Handwerger
Funding acquisition: Jeffrey S. Munroe, Alexander L. Handwerger
Investigation: Jeffrey S. Munroe, Benjamin J. C. Laabs, Lee B. Corbett
Methodology: Jeffrey S. Munroe, Lee B. Corbett
Project administration: Jeffrey S. Munroe
Resources: Jeffrey S. Munroe, Lee B. Corbett
Validation: Jeffrey S. Munroe
Visualization: Jeffrey S. Munroe
Writing – original draft: Jeffrey S. Munroe
Writing – review & editing: Jeffrey S. Munroe, Benjamin J. C. Laabs, Lee

Abstract Rock glaciers are common in alpine landscapes, but their evolution over time and their significance as agents of debris transport are not well-understood. Here, we assess the movement of an ice-cemented rock glacier over a range of timescales using GPS surveying, satellite-based radar, and cosmogenic ^{10}Be surface-exposure dating. GPS and InSAR measurements indicate that the rock glacier moved at an average rate of ~10 cm yr^{-1} in recent years. Sampled boulders on the rock glacier have cosmogenic surface-exposure ages from 1.2 to 10 ka, indicating that they have been exposed since the beginning of the Holocene. Exposure ages increase linearly with distance downslope, suggesting a slower long-term mean surface velocity of 3 ± 0.3 cm yr^{-1}. Our findings suggest that the behavior of this rock glacier may be dominated by episodes of dormancy punctuated by intervals of relatively rapid movement over both short and long timescales. Our findings also show that the volume of the rock glacier corresponds to ~10 m of material stripped from the headwall during the Holocene. These are the first cosmogenic surface-exposure ages to constrain movement of a North American rock glacier, and together with the GPS and satellite radar measurements, they reveal that rock glaciers are effective geomorphic agents with dynamic multi-millennial histories.

Plain Language Summary Rock glaciers are slowly moving mixtures of ice and rock debris found in many cold mountain environments. Although they are common, questions remain about their rates of movement, age, and effectiveness in shaping mountain landscapes. We studied a typical rock glacier in the Uinta Mountains of Utah (USA), demonstrating that it formed about 10,000 years ago and is currently moving at a rate of about 10 cm per year. This is about 3 times faster than the long-term average calculated from the age and length of the rock glacier, meaning that it is now moving faster than usual. We were also able to estimate that this rock glacier is transporting a volume of debris equivalent to about 10 m of erosion from the cirque headwall above it, confirming that rock glaciers, although slow moving, are important agents of erosion.

1. Introduction

Rock glaciers are mixtures of ice and rock debris common in high mountain environments (Giardino et al., 1987). Considerable research has focused on rock glacier genesis, revealing that some are ice-cemented features formed as meltwater infiltrates and freezes within talus (Wahrhaftig & Cox, 1959). In contrast, rock glaciers with a massive ice core appear to originate from alpine glaciers that are completely buried by supraglacial debris (Barsch, 1987). In many cases, both of these end-member processes are likely involved in varying degrees (Berthling, 2011). Regardless of their origin, their genetic connection with permafrost and ice makes rock glaciers important sources of (paleo)climatic information (Janke, 2007; Konrad et al., 1999; Moran et al., 2016), and their movement suggests that they may be significant geomorphic agents in high mountain landscapes (Anderson et al., 2018; Giardino & Vitek, 1988). Previous studies have also highlighted the possibility that rock glaciers and their immediate surroundings may serve as refugia for cold-adapted organisms in the face of warming alpine climates (Brighenti et al., 2021; Green et al., 2022; Hotaling et al., 2017, 2020). An additional line of active research on rock glaciers is their role as sources of water to high-elevation hydrologic systems (Janke et al., 2017; Jones et al., 2019; Rangecroft et al., 2015; Wagner et al., 2021; Winkler et al., 2016).

Despite this expansive body of research, fundamental questions remain about rock glacier evolution and behavior, such as when they originated during the post-glacial interval (Amschwand et al., 2021), how variable their

B. Corbett, Paul R. Bierman, Alexander L. Handwerger

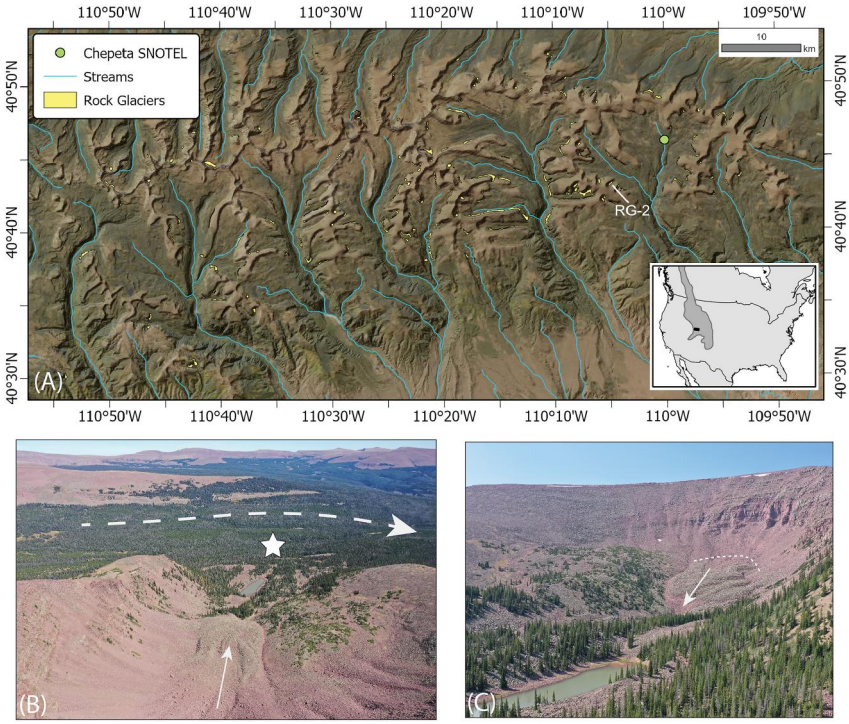

Figure 1. Location of the study area. (a) True color satellite image of the Uinta Mountains from Earthstar Graphics. Active rock glaciers identified through satellite InSAR analysis are shown in yellow (Brencher et al., 2021). The location of RG-2 is highlighted. Green circle marks the Chepeta SNOTEL site. Inset shows the position of the map (black rectangle) within the Rocky Mountain system (dark gray) in western North America. (b) View northeastward over RG-2 from an uncrewed aerial vehicle (UAV) flying at an altitude of ~3,800 m. White arrow emphasizes the direction of movement. Thicker dashed arrow illustrates the flow direction of the former glacier in the West Fork Whiterocks valley during the Last Glacial Maximum (Munroe & Laabs, 2009). White star designates the position of the two glacial erratics sampled from the lip of the cirque for cosmogenic surface-exposure dating. (c) View southward over RG-2 from a UAV flying at an altitude of ~3,400 m. White arrow emphasizes the direction of movement. Thin dashed line highlights the approximate boundary between the active talus and the rock glacier. Bedrock cliffs in the headwall above the rock glacier are clearly visible.

velocities are over time (Bertone et al., 2023; Krainer & He, 2006; Lambiel & Delaloye, 2004), and what climatic variables influence their rates of movement (Cicoira et al., 2019; Kääb et al., 2007; Kenner et al., 2017). Improved understanding of rock glacier genesis is germane to the use of rock glaciers as paleoclimate indicators (Charton et al., 2021; Millar & Westfall, 2008), and better constraints on rock glacier age and rates of movement are relevant to models of post-glacial evolution of mountain landscapes (Anderson et al., 2018; Knight et al., 2019).

Here, we employ ground-based GPS surveying, satellite remote sensing, and cosmogenic surface-exposure dating to characterize the motion of a typical rock glacier in the Uinta Mountains of northeastern Utah, a portion of the U. S. Rocky Mountains (Figure 1). Rock glaciers are abundant in this area, but their age is unknown, their movement over time has not been quantified, and their geomorphic significance has not been assessed. We use our results to test the hypothesis that a representative rock glacier formed during the Little Ice Age, to compare modern and long-term surface velocities, and evaluate its significance as a geomorphic agent.

2. Setting

The Uinta Mountains (Figure 1) host nearly 400 rock glaciers (Munroe, 2018) on account of a periglacial climate suitable for the persistence of alpine permafrost (Obu et al., 2019), and layered meta-sedimentary bedrock featuring bedding planes and joints vulnerable to exploitation by freeze-thaw weathering (Bradley, 1995). Roughly 85% of these rock glaciers are lobate features wider than they are long, and the remainder are tongue-shaped rock glaciers on cirque floors. Satellite-based interferometric synthetic aperture radar (InSAR) analysis reveals that 205 of the rock glaciers in the Uinta Mountains were moving between 2016 and 2019 (Brencher et al., 2021). Prior work proposed that rock glaciers in these mountains might be the lingering geomorphic

signature of cooler, snowier conditions during the Little Ice Age (Munroe, 2002) that depressed alpine treeline (Munroe, 2003), accelerated rates of talus production, and facilitated the survival of snowbanks through the summer. On the other hand, a study of a lacustrine sediment core suggested that one rock glacier was active in multiple pulses during the late Holocene (Munroe et al., 2013).

We focused on a rock glacier (Figure 1, video in supplement) designated as "RG-2" in a previous work (Munroe, 2018; Munroe & Handwerger, 2023a, 2023b) because the fresh appearance of ridges and furrows on its surface and the steepness of its lateral slopes imply recent motion (e.g., Baroni et al., 2004). RG-2, which is comprised of angular quartzite blocks up to 5-m in diameter, is ∼500 m long, has terminal and side slopes more than 20 m tall, is located at an average elevation of ∼3,350 m, and discharges 0°C water in late summer sourced from the melting of internal ice (Munroe, 2018; Munroe & Handwerger, 2023a, 2023b). The headwall behind RG-2 is ∼400 tall m, reaching an elevation of ∼3,800 m. The mean annual air temperature at the Chepeta SNOTEL site, <10 km to the north at an elevation of 3,200 m (Figure 1), is 1.0°C, with a mean annual precipitation of ∼775 mm (National Water and Climate Center, 2024).

3. Methods

3.1. UAV Mapping

A set of 244 vertical photographs collected by an uncrewed aerial vehicle (UAV) with internal GPS was used to produce a high-resolution photomosaic of RG-2. Photographs overlapped 80% in both the along track and cross track directions, and were collected at a constant altitude of 130 m above the ground surface over an area of 45 ha. Images were processed with Maps Made Easy to yield a mosaic with a resolution of 2.8 cm per pixel. Structure from Motion (SfM) analysis was implemented to generate a digital elevation model (DEM) for the rock glacier surface with an average resolution of 10 cm.

3.2. Real-Time Kinematic (RTK) GPS

Motion of RG-2 was quantified with a pair of Emlid Reach RTK-GPS units and a network of 32 points established in September 2021. Marks were made on the flat surfaces of prominent boulders using a hand drill. These points were resurveyed in September 2022 to yield annual displacement vectors. Measurements were collected by averaging over 5 s; each has an estimated error <1 mm.

The base station for the GPS survey was set up ∼550 m from the front of RG-2 and surrounded by 4 control points on stable boulders. Repeat surveying of these points yielded apparent displacements of <2 cm, defining the error inherent in reestablishing the base station over the reference point. During post-processing, the X and Y errors for the repeat survey were calculated for all 4 reference points, and these average errors were subtracted from the survey points on the rock glacier to yield corrected X-Y coordinates.

3.3. Satellite-Based Interferometric Synthetic Aperture Radar (InSAR)

We measured multi-year motion of RG-2 using InSAR time series generated from open-access SAR data (Alaska Satellite Facility, 2024) acquired by the Copernicus Sentinel-1 A/B satellites in the interferometric wide (IW) swath mode on ascending track 122 between 2016 and 2021 (Table S1). Interferogram pairs were constructed using the Jet Propulsion Laboratory InSAR Scientific Computing Environment (ISCE) version 2 software (Rosen et al., 2012). To reduce noise and improve interferometric coherence, we multilooked the SAR images using 5 looks in range and 1 look in azimuth, resulting in a ∼12 m by 15 m pixel size. Topographic contributions to the phase were removed using the Shuttle Radar Topography Mission (SRTM) digital elevation model (Farr et al., 2007). To avoid issues related to snow-cover on the rock glacier surface, we employed an established strategy (see details in Brencher et al., 2021), which involved processing short timespan snow-free pairs during the summer period and longer timespan pairs that connect snow-free periods. In total, we processed 108 interferograms (Table S1).

A time series inversion was performed on the unwrapped interferogram pairs using the open-source Miami INsar Time-series software in the PYthon (MintPy) software package (Yunjun et al., 2019). We excluded pixels with coherence less than 0.7 and made additional corrections including linear deramping, tropospheric phase corrections with the European Center for Medium-Range Weather Forecasts (ECMWF) ERA-5 reanalysis data set (Jolivet et al., 2011), and DEM error corrections (Fattahi & Amelung, 2013). We projected the line-of-sight (LOS)

displacement onto the average downslope direction (assuming surface-parallel motion) of the rock glacier using standard methods (see details in Brencher et al., 2021; Liu et al., 2013). The downslope projection can provide displacement values that are closer to the magnitude of the true 3D motion. For RG-2, the downslope projection scaling factor is approximately −3.8.

Lastly, we quantified uncertainty in the InSAR-derived surface movement of RG-2 by measuring the apparent displacement in a nearby stable area. For this exercise, we selected a 0.025-km^2 region along a ridgetop approximately 800 m east of RG-2.

3.4. Cosmogenic Surface-Exposure Dating

Rock samples were collected from six prominent boulders on the surface of RG-2 (Figure 2a, Figures S1–S6 in Supporting Information S1), and two additional samples were taken from glacial erratics at the lip of the cirque 900 m downslope from the rock glacier front (Figure 1b, Figures S7 and S8 in Supporting Information S1). Samples were collected by cutting parallel strips of rock with an angle grinder and using a hammer and chisel to dislodge the pieces. Topographic shielding was measured for the location of each sample at 10° intervals to compute a shielding factor applied to the production rate at each sample site. The shielding factor was computed using expressions modified from standard methods (Gosse & Phillips, 2001).

Quartz was isolated and purified at the North Dakota State University Cosmogenic Nuclide Preparation Lab. Rock samples were reduced by crushing and milling, and the 250–500 μm grain size range was recovered by sieving. Magnetic grains were removed with a neodymium hand magnet, and the remaining quartz grains were repeatedly etched in dilute hydrofluoric and nitric acids to yield purified quartz following standard methods (Kohl & Nishiizumi, 1992).

Beryllium extraction occurred at the University of Vermont Community Cosmogenic Facility using established methods (Corbett et al., 2016). Samples were prepared in a single batch which included 8 unknowns, one blank, and one reference material, UVM-A (Corbett et al., 2019). We added ∼250 μg of ^{9}Be to each sample using an in-house carrier with a concentration of 304 ppm (Table S2). We corrected sample ratios for backgrounds using the batch blank, $4.4 \pm 0.9 \times 10^{-15}$, and propagated the blank uncertainty in quadrature.

We analyzed ^{10}Be/^{9}Be ratios by Accelerator Mass Spectrometry at the Purdue Rare Isotope Measurement Laboratory (PRIME). Samples were normalized to the primary standard 07KNSTD3110 with an assumed ratio of $2{,}850 \times 10^{-15}$ (Nishiizumi et al., 2007). Sample ratios (Table S2) ranged from 0.6 to 7.0×10^{-13}, with an average analytic uncertainty of 3.3 ± 1.6% (1SD, $n = 8$).

We calculated exposure ages using version 3.0 of the online exposure age calculator (Balco, 2008 http://hess.ess.washington.edu/math/). Site-specific ^{10}Be production rates were calculated with the Lifton-Sato-Dunai nuclide dependent ("LSDn" Lifton et al., 2014) scaling model and two calibration data sets: (a) in situ ^{10}Be data from the independently dated surface at the Promontory Point, Utah production-rate calibration site (Lifton et al., 2015), and (b) a global calibration data set (Borchers et al., 2016). Ages reported in the text are based on the production rate calibrated from Promontory Point due to its proximity of this calibration site to our study area. We note that these ages are ∼200–300 yr younger than those computed using the global calibration data set. No correction was made for snow-shielding because the height of the sampled boulders above the surrounding rock glacier surface suggests they were windswept, which likely minimized snow cover. Nonetheless, the potential for some small degree of snow shielding does introduce the possibility that the reported ages are slight underestimates. In our age calculations, we made no correction for nuclides that may have been inherited from periods of prior exposure on the headwall, which would result in exposure ages greater than the true age of the rock glacier surface. While the short distance of boulder transport from the headwall minimizes boulder rounding and removal of inherited nuclides, we found no evidence of old outliers or other signals of nuclide inheritance in the set of exposure ages. Furthermore, given the large size of the sampled boulders (>2 m in diameter) and the low probability that boulder tops were exposed prior to deposition atop the rock glacier, it is unlikely that the nuclide inventories we measured could exist for a rock glacier originating during the Little Ice Age.

3.5. Ground Penetrating Radar

To investigate the internal structure of RG-2, a ground penetrating radar (GPR) survey with a GPS-enabled GSSI SIR-4000 control unit driving a 100-MHz antenna was conducted in early September along a 90-m transects

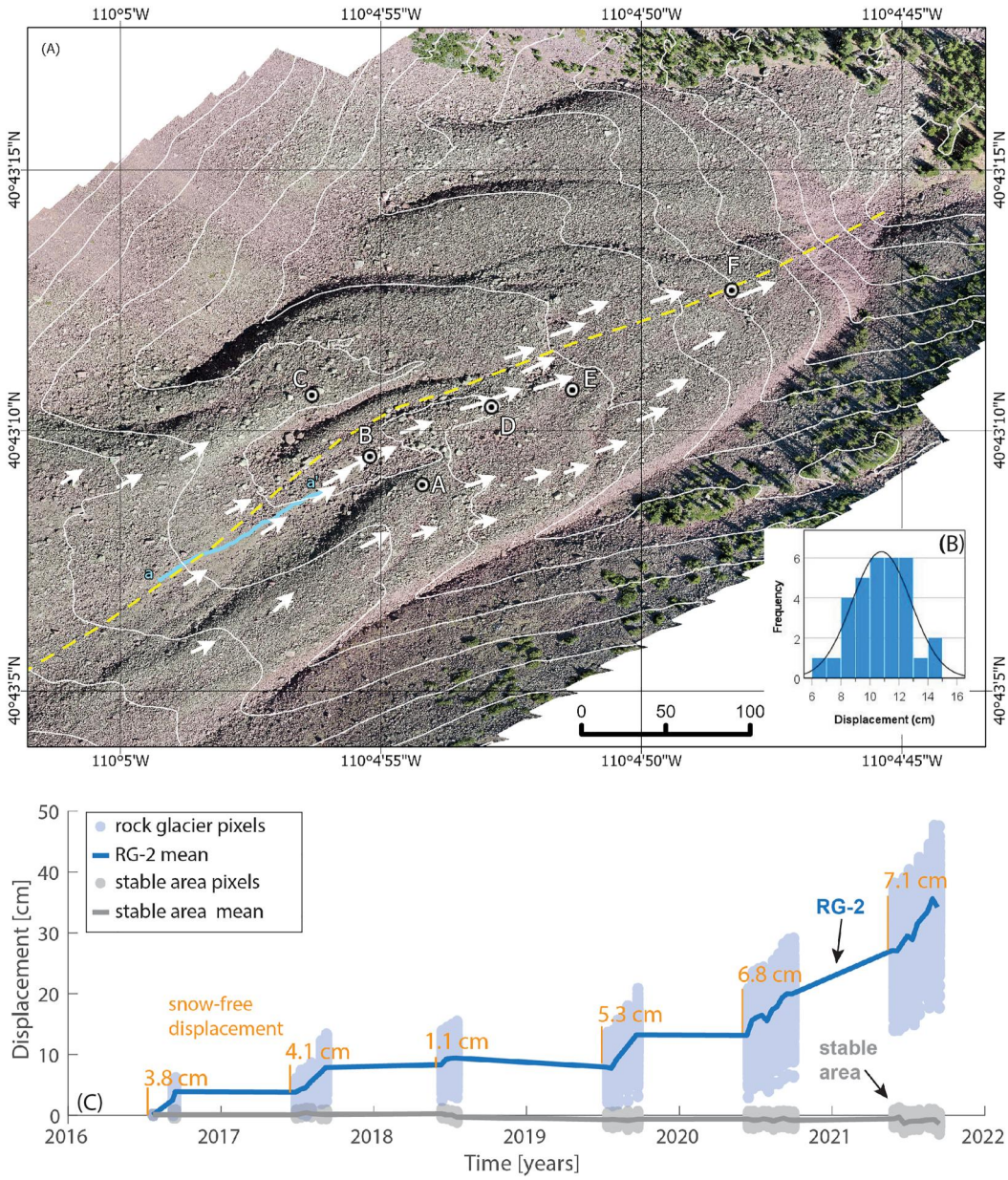

Figure 2. (a) True color orthophoto mosaic of RG-2 with 10-m contours (thin white lines) constructed from georeferenced images obtained by a UAV. The rock glacier is moving to the east-northeast. Vectors present the displacement of 32 points between September 2021 and September 2022. The scale of the vectors is 100× the map for clarity. The yellow dashed line delineates the longitudinal profile in Figure 5. The blue line a-a' marks the GPR transect shown in Figure 6. The points A-F are cosmogenic surface-exposure samples, keyed to Table 1 and Figures 5 and 7. Panel (b) presents the histogram of annual displacement values showing a normal distribution around a mean of 10.8 cm. Panel (c) presents displacement time series of RG-2 from 2016 through 2021. Dark blue line shows spatial mean value, whereas light blue dots show individual pixel values within RG-2. The dark gray line shows the spatial mean of a stable ridgetop, and the light gray dots show individual pixels within the stable area. The InSAR line-of-sight motion was projected onto the average downslope direction of the rock glacier. Quantification of surface displacement during the winter is not possible due to the complicating effects of snow cover.

parallel to the longitudinal axis in the rooting zone of the rock glacier (Figure 2a). The rough surface of most of RG-2 limited GPR surveying to this upper area where boulder frequency was reduced compared to the rest of the landform. The antenna was carried along a 300-foot non-metallic tape between two operators who suspended it ~20 cm above the ground surface. We acknowledge that this technique may have reduced radar penetration and

produced complex diffraction patterns (Merz et al., 2015), but it was necessary to maintain a constant orientation of the antenna with respect to the ground surface. The GPR was configured to collect 1,024 samples per scan over a range of 650 ns. 93 scans were made per second, and GPS coordinates were automatically added every 2 s. Marks manually recorded in the GPR datafile every 30 feet were used to enforce a real-world horizontal scale during post-processing.

Processing of the GPR data in Radan 7.6.19 included aligning the first pulse of the radargram with the ground surface to correct for elevating the antenna, implementation of an exponential range gain to accentuate deeper reflectors, a vertical infinite impulse response (IIR) filter to reduce noise, a boxcar stacking finite impulse response (FIR) filter to clarify stratigraphy, a second vertical IIR filter followed by a second round of exponential range gain to even out reflector amplitudes, distance normalization to convert the data to a constant horizontal scale, and topographic normalization based on the GPS data.

Although the radar velocity within RG-2 is not directly known, work on a similar feature derived a value of 0.12 m ns^{-1} (Degenhardt et al., 2003), corresponding to a relative permittivity (ε_r) of 6, which is typical for permafrost (Reynolds, 2011). Applying this value to RG-2 converts the two-way travel time of the radar waves to estimated depth, and suggests that structures within RG-2 are resolvable to a depth of ∼20 m, with a vertical resolution of ∼0.3 m (Reynolds, 2011). Application of a different ε_r value would change the apparent depth of stratigraphy observed in the GPR results but would not impact our primary goal of using the GPR to evaluate whether RG-2 has a massive ice core.

3.6. Estimation of Headwall Recession Rate

We estimated the volume of debris (in m^3) comprising RG-2 by multiplying the average rock glacier thickness derived from the topographic data from the UAV by the plan-view surface area of the landform, and assuming a porosity of 30% (Arenson & Jakob, 2010; Jones et al., 2019; Wahrhaftig & Cox, 1959). Dividing this debris volume by the time span demonstrated by the cosmogenic exposure results yielded a delivery rate of rock debris from the headwall to RG-2 (in m^3 yr^{-1}). The area of the headwall above RG-2 (in m^2) was calculated in Google Earth. Dividing the rate of debris delivery by this area generated an estimate for the rate of erosion through freeze-thaw weathering and rock fall (in m yr^{-1}). Extrapolation of this rate over the age of RG-2 produced an estimate of total headwall recession (in m).

4. Results

Our repeat RTK-GPS survey reveals that boulders on the surface of RG-2 exhibit quantifiable downslope motion. All 32 points established in September 2021 were unambiguously relocated and resurveyed in September 2022. Each was displaced in a coherent downslope manner by an amount ∼3× greater than the uncertainty quantified by relocating stable reference points near the base GPS station. Displacements of individual boulders ranged from 6.2 to 14.9 cm (Figure 2b) exhibiting a normal distribution ($p = 0.964$, Shapiro-Wilk test) around a mean of 10.8 ± 2 cm. Boulders located along the longitudinal axis of the rock glacier generally exhibited slightly greater displacements (Figure 2a).

The downslope displacement of the rock glacier surface quantified by satellite InSAR analysis confirms the velocities revealed by the GPS surveying and also reveals temporal variability. The InSAR measurements, which are limited to snow-free periods, demonstrate seasonal increases in surface motion (Figure 2c) with a range of velocities from 10.7 to 29.6 cm yr^{-1} when summer measurements are extrapolated for 12 months (Figure 3). The mean cumulative downslope displacement estimated for the entire rock glacier over 6 years was 34 cm ± 5 cm (± standard deviation), with mean annual displacements between 3.8 and 7.1 cm (Figure 2c). The mean cumulative displacement of the nearby stable region (Figure 4), which is used to approximate the InSAR uncertainty, was −1.5 ± 0.5 cm (± standard deviation), which is significantly lower than the displacement of RG-2 over the same time period. At the scale of the entire interferogram, RG-2 is obvious as a discrete oval zone of consistently higher velocities that contrasts strongly with the movement pattern of the surrounding landscape (Figure 4).

The six samples collected from boulders on the rock glacier surface yielded ^{10}Be exposure ages from 1.2 to 10.0 ka (Table 1 and Table S2). Although not all samples were collected along the longitudinal axis of RG-2, all but one (RG-2-5) were taken from the crests of arcuate ridges that bulge downslope in the rock glacier center, and trail backward along the sides (Figure 2a). When the exposure ages (excepting RG-2-5) are plotted as a function of the

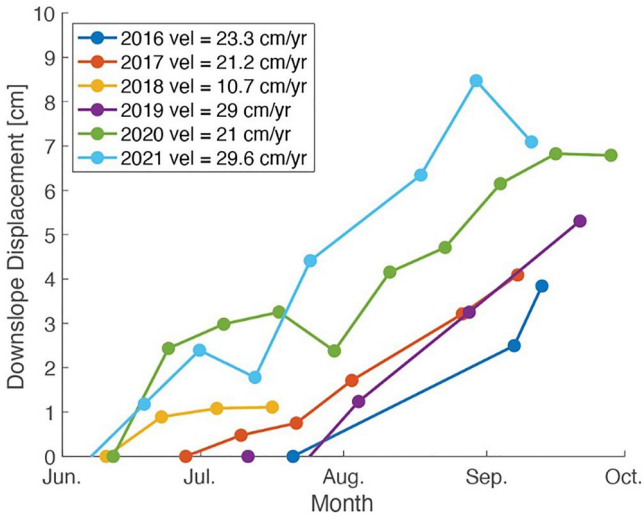

Figure 3. InSAR displacement time series for RG-2 for 6 different snow-free seasons. The lines show the spatial mean for RG-2. To highlight the seasonal variability, we plot the cumulative displacement snow-free period starting at 0. Measured InSAR line-of-sight displacement was projected onto the downslope direction of the rock glacier. Velocities are calculated using linear fits to the displacement time series, and are extrapolated to 12 months. Note that some years (e.g., 2016 and 2018) have few snow-free InSAR measurements and that motion of RG-2 is primarily limited to the summer season.

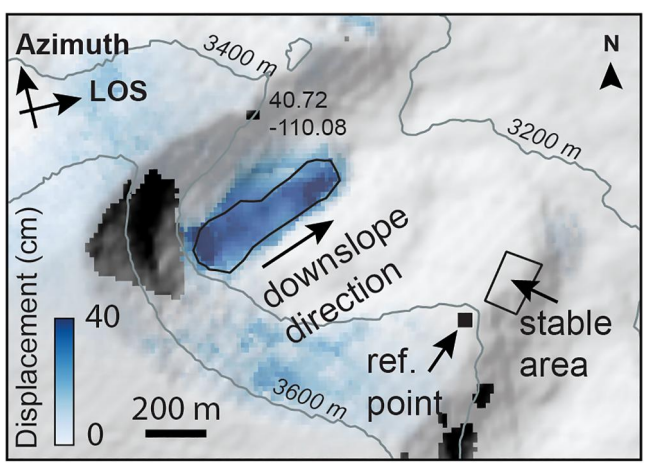

Figure 4. Interferogram showing focused displacement (darker blue) within the polygon defining the mapped boundaries of RG-2. Azimuth notes the direction of flight of the satellite; LOS designates the line-of-sight direction of the radar, which is nearly parallel to the downslope direction. The stable reference point used for InSAR processing is noted in the lower right. Dark gray areas to the west of the rock glacier are steep parts of the cirque headwall that were not imaged by the satellite radar.

position of their corresponding ridge along the longitudinal axis of RG-2, they display an overall pattern of increasing exposure age with distance downslope. This pattern of exposure ages exhibits a linear relationship with a slope of 30 yr m^{-1}, corresponding to an average Holocene displacement rate of ~3 ± 0.3 cm yr^{-1} (Figure 5). Sample RG-2-5 (E in Table 1) is an exception to this overall pattern, with an anomalously young age of 1.2 ka despite its position as the second most distal boulder sampled (Figure 5).

The GPR data reveal resolvable layering at all depths, with many layers spanning >10 m horizontally and an internal stratigraphy characterized by wavy folding and local unconformities (Figure 6). Radar reflections are generally faint in the upper ~2 m, beneath which a sharp transition to higher-amplitude reflectors is apparent. This zone of prominent reflections is ~5 m thick and continuous along the length of the transect. Below a depth of ~7 m, reflections are less prominent, but stratigraphy is still resolvable. Notable features include long-wavelength folds, local onlapping relationships, and convex-up features resembling the "nested spoons" structures noted in previous work (Petersen et al., 2020). No clear contact between the rock glacier and underlying bedrock is observed, likely because the necessary suspension of the antenna above the ground surface limited the ultimate depth of penetration.

The lateral continuity of reflectors, dipping reflectors, expressions of folding, and angular unconformities suggest that the GPR results are less compromised by effects related to the rough rock glacier surface than some previous efforts (e.g., Merz et al., 2015). This outcome may be due to the antenna frequency utilized or to the ability to keep the antenna stable afforded by hovering it slightly above the surface. Even though the base of the rock glacier was not successfully imaged, the GPR data are sufficient for assessing whether the interior of RG-2 is radar transparent/ice-cored (e.g., Petersen et al., 2020) or composed of resolvable ice-cemented layers (e.g., Degenhardt et al., 2003).

5. Discussion

Our approach combining RTK-GPS surveying, satellite InSAR, cosmogenic surface-exposure dating and GPR provides insights into the origin of RG-2, refutes the hypothesis that it formed during the Little Ice Age, and reveals that it has transported considerable rock debris over time. Additionally, comparing short-term and long-term displacement measurements indicates that RG-2 exhibits kinematic variability over seasonal, yearly, and likely millennial timescales.

Our measurements from GPS and InSAR demonstrate that the surface of RG-2 is currently moving at ~10 cm yr^{-1} with temporal variations over seasonal and annual (and likely longer) timescales. Similar patterns were reported by other studies (e.g., Haeberli, 1985; Konrad et al., 1999; Krainer et al., 2015), and investigations have suggested that variations in shear strength, temperature and water availability drive these changes (Bertone et al., 2023; Kenner et al., 2017, 2020; Nickus et al., 2015). The overall velocities for RG-2 are at the lower range of values reported for rock glaciers around the world (Janke et al., 2013; Krainer & He, 2006). We hypothesize that RG-2 may be moving slower because the lack of an ice core and/or the drier climate reduces the amount of water reaching the basal shear zone where motion is focused (Ikeda et al., 2008; Kenner et al., 2017, 2020; Wirz et al., 2016).

Our cosmogenic exposure results demonstrate that RG-2 originated shortly after local deglaciation and has increased in length over time. The two glacial

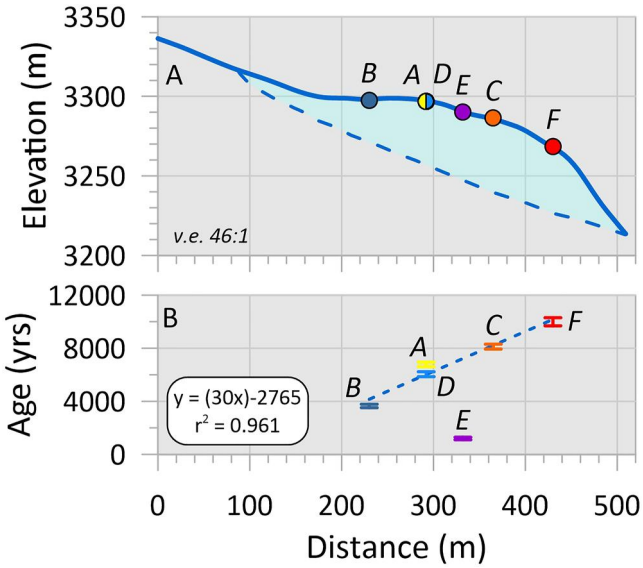

Figure 5. (a) Topographic profile along RG-2 extracted from the DEM produced from the UAV data (v.e. is vertical exaggeration). The dashed line denotes the base of the rock glacier inferred from the continuation of the valley slope. Circles mark the intersection of the longitudinal profile shown in Figure 2, with ridges on the rock glacier surface corresponding with cosmogenic surface-exposure ages. Samples A and D were collected from the same ridge. Colors correspond with sample locations in Figure 7. (b) Plot of exposure ages (with 2-sigma uncertainties) as a function of the distance of their corresponding ridge along the topographic profile. Ages except the outlier (E, purple) are fit with a linear function with a slope of 30 yr m^{-1} corresponding to movement at a rate of ~3 cm yr^{-1}.

erratics from the lip of the cirque below RG-2 (Figure 1b, Figures S7 and S8 in Supporting Information S1) have overlapping ^{10}Be exposure ages averaging 14.2 ± 0.7 ka (Table 1 and Table S2). These ages are consistent with the basal ^{14}C age of 10,800 ± 120 yrs (12.7 ka BP) determined for a tarn 7 km away at the head of the valley to which the cirque occupied by RG-2 is a tributary (Munroe & Laabs, 2017). Retreat of the alpine glacier in this drainage (Figure 1b) and local deglaciation, therefore, occurred in the latest Pleistocene, giving way to periglacial conditions under which RG-2 originated sometime before 10.2 ka (Figure 7), the oldest ^{10}Be age on the rock glacier surface (Scapozza et al., 2014). Subsequent growth of RG-2 reflects extension of the feature as a conveyor belt (Anderson et al., 2018; Kääb & Reichmuth, 2005), as revealed by the linear relationship between exposure age and the position of the surface ridges along which the ^{10}Be samples were collected (Figure 5). In this model, debris is added to the rooting zone of RG-2 as rock falls from the headwall (Figure 1c), and the entire rock glacier extends downslope over time (Figure 7). Ridges on the rock glacier surface may be formed from material delivered by large magnitude mass wasting events (Kenner et al., 2014), through folding and thrusting during movement (Florentine et al., 2014; Frehner et al., 2015; Kääb & Weber, 2004), or they might reflect reactivation of previously stable parts of the rock glacier that proceed to override stationary areas (Amschwand et al., 2021). Overall, from the spatial and temporal pattern of the surface-exposure ages we generated, we conclude that RG-2 did not form during the Little Ice Age, which culminated in this region during the 17th Century (Naftz et al., 1996); rather, it has been transporting material and extending downvalley for millennia (Figure 7).

Progressive growth of RG-2 over more than 10,000 years (Figure 7) corroborates multi-millennial ages for rock glaciers reported from ^{14}C dating of organic remains (Konrad et al., 1999; Krainer et al., 2015), from semi-quantitative Schmidt Hammer measurements (Rode & Kellerer-Pirklbauer, 2012), and from other investigations that employed surface-exposure dating (Amschwand et al., 2021; Lehmann et al., 2022). Although studies have suggested that boulders on rock glaciers may inherit cosmogenic nuclides from prior exposure (e.g., Çiner et al., 2017), the similarity of the ages we determined for the glacial erratics (Table 1), both with each other and with independent estimates of deglaciation in this valley (Munroe & Laabs, 2017), argues for limited ^{10}Be inheritance in this geomorphic system (cf. Amschwand et al., 2021), as does the linear relationship between age and projected position along the longitudinal axis (Figure 5). The anomalously young exposure age of boulder E (RG-2-5, Table 1) suggests that this boulder may have been overturned during transport or delivered from depth to the rock glacier surface due to compressive flow.

Table 1
Cosmogenic Surface-Exposure Samples and Results

Code[a]	Sample	Latitude (DD.ddd)	Longitude (DD.ddd)	Elevation (m)	Thickness (cm)	Shielding	^{10}Be age[b] (yr)	^{10}Be uncertainty (yr)
A	RG-2-1	40.719160	−110.081719	3,312	1.8	0.9668	6,780	310
B	RG-2-2	40.719311	−110.081998	3,309	1.8	0.9624	3,650	190
C	RG-2-3	40.719637	−110.082307	3,312	2.1	0.9603	8,130	360
D	RG-2-4	40.719575	−110.081350	3,308	1.8	0.9730	6,050	290
E	RG-2-5	40.719666	−110.080919	3,300	1.8	0.9727	1,200	100
F	RG-2-6	40.720198	−110.080069	3,275	1.8	0.9747	10,000	480
G	RG-2-7	40.726215	−110.071853	3,170	1.8	0.9927	14,310	680
H	RG-2-8	40.726209	−110.071662	3,169	1.8	0.9927	14,000	600

[a]Linked to Figure 2. [b]Ages and uncertainties rounded to nearest 10. Unrounded values are presented in Table S1.

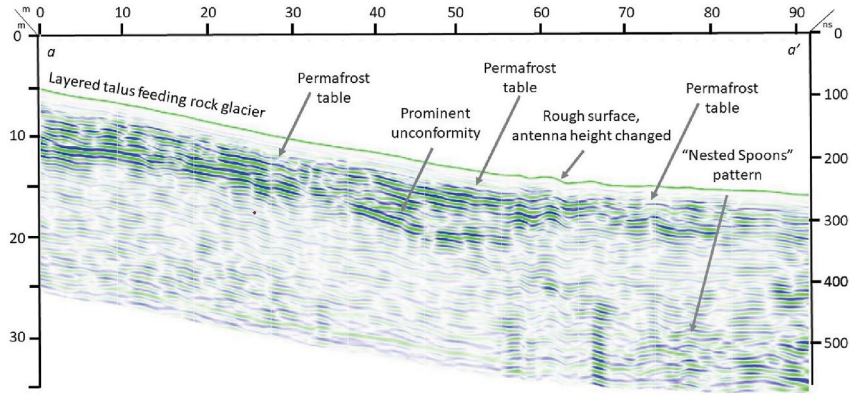

Figure 6. Longitudinal GPR transect along the blue line a-a' in Figure 2. Depths are estimated using a relative permittivity (ε_r) of 6, which is typical for permafrost (Reynolds, 2011).

The modern surface velocity estimates from 1 year of RTK-GPS measurements and 6 years of InSAR analysis, and the long-term rate from the cosmogenic surface-exposure ages reveal complex temporal kinematics. The InSAR time series, in which the highest velocities were observed between 2020 and 2022 (Figure 2c), suggests that RG-2 may be accelerating, perhaps in the early phases of a destabilization cycle currently characterizing some rock glaciers in the Alps (Marcer et al., 2021). Alternatively, RG-2 may spend much of its time dormant, only

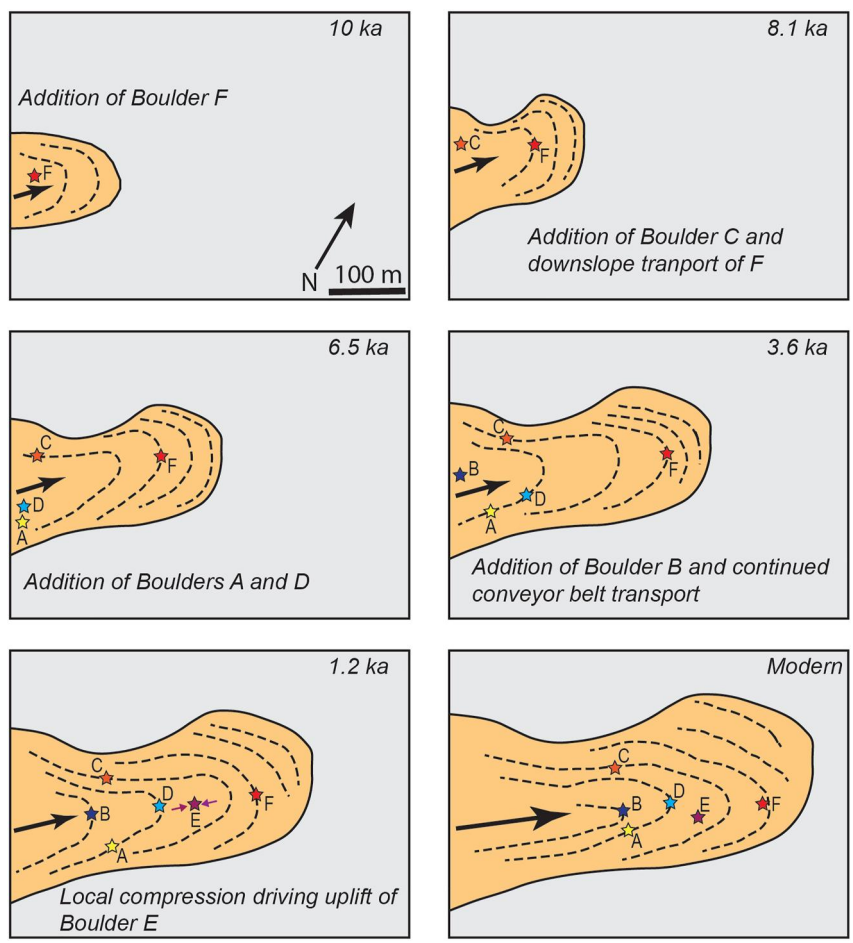

Figure 7. Schematic maps presenting the evolution of RG-2 during the Holocene. Dashed lines mark prominent compression ridges.

occasionally reactivating to move at rates of ~10 cm yr^{-1}. Modern observations, therefore, happened to catch RG-2 in an active phase, whereas our long-term rate reflects an overall average, analogous to the Sadler Effect in stratigraphic sequences, which postulates that apparent rates of sedimentation decrease when averaged over longer time intervals (Sadler, 1981).

Similar models of general stability punctuated by episodes of relatively rapid movement have been inferred for the ice-cored Lazaun rock glacier in Italy (Krainer et al., 2015) as well as for ice-cemented rock glaciers in the French Alps (Lehmann et al., 2022) and in Switzerland (Amschwand et al., 2021). Oscillations between dormancy and activity might be climatically forced if conditions alternately lead to the formation and ablation of segregation ice lenses within the debris matrix comprising RG-2 (Wayne, 1981) or by shifts in permafrost microclimate that alter the pathways by which water moves through the rock glacier interior (Kenner et al., 2017, 2020). The number of ^{10}Be ages we generated is not sufficient to confirm whether RG-2 oscillated through discrete periods of motion and inactivity (cf. Amschwand et al., 2021; Lehmann et al., 2022), and our samples were not collected over the entirety of the rock glacier surface due to safety considerations during fieldwork. However, the overall length of RG-2 (~500 m) and its apparent age of >10 ka are incompatible with continuous movement at the average modern rate of ~10 cm yr^{-1}, which would have produced a feature ~1 km long. The current velocity is therefore not representative of the average rate at which the surface of RG-2 has moved over millennial-scale time periods.

The results from GPR surveying provide insight into the internal structure of RG-2. We interpret the reflector at a depth of ~2 m as the permafrost table, marking the transition from open-work quartzite rubble above to ice-cemented material below (Figure 6). This interpretation could not be confirmed directly in the field due to the impossibility of excavating into the rock glacier by hand. However, the persistence of this pronounced reflector along the profile implies the presence of a laterally continuous change in radar reflectivity at that depth, and an active layer thickness of ~2 m at the end of the summer is consistent with geophysical investigations and direct observations on rock glaciers in numerous mountain ranges (Degenhardt & Giardino, 2003; Degenhardt et al., 2003; Florentine et al., 2014; Potter, 1972). Below this depth, we interpret the apparent stratigraphy in the GPR results as evidence of crude layering defined by varying proportions of debris and ice (Figure 6). Without direct observation from boreholes it is not possible to evaluate this interpretation; however, drilling in other rock glaciers has demonstrated a similar internal stratigraphy (Arenson et al., 2002; Krainer et al., 2015; Monnier & Kinnard, 2013; Mühll & Holub, 1992).

Overall, the resolvable layering in the GPR surveys suggests that RG-2 formed as segregation ice accumulated from water infiltrating talus (Degenhardt, 2009; Degenhardt & Giardino, 2003; Wayne, 1981). Significantly, radar results do not express the characteristic reflection-free clarity seen in GPR data from rock glaciers with an ice core (Petersen et al., 2020). Although the entire length of RG-2 could not be surveyed (Figure 2), the most likely place for massive ice is near the rock glacier rooting zone where the transect was collected, because this is where ice and snow are added to the system (Janke et al., 2013). Therefore, we infer that at least the upper part of RG-2 is ice-cemented, and that the landform did not evolve as a cirque glacier that became progressively buried in debris (Anderson et al., 2018).

The interpretation that RG-2 is likely ice-cemented allows us to estimate the total volume of the feature in order to evaluate its efficacy as a geomorphic agent over time. An elevation profile along the central axis, based on the topographic data collected by the UAV, suggests that RG-2 is a convex-up body with an average thickness of ~28 m superimposed on a sloping valley floor (Figure 5), an estimate that is consistent with the height of the rock glacier front and side slopes and the lack of a clear basal reflector in the longitudinal GPR profile. Given a surface area of 9.4×10^4 m^2, an average thickness of 28 m, and an assumption of 30% porosity, a value consistent with previous estimates (Arenson & Jakob, 2010; Jones et al., 2019; Wahrhaftig & Cox, 1959), a rough estimate for the volume of debris comprising RG-2 is 1.84×10^6 m^3. For an age of 10 ka years, this corresponds to a debris delivery rate of ~190 m^3 yr^{-1}. Exposed bedrock on the headwall above RG-2 (Figure 1c) has an area of ~2.0×10^5 m^2, thus the rate of erosion through freeze-thaw weathering and rock fall is 0.94 mm yr^{-1} and the headwall has retreated on the order of 10 m over the Holocene. This estimate is crude given the lack of firm constraints on rock glacier thickness and the need to assume a relevant porosity value. Nonetheless, this rate is similar to values estimated for rock glacier-related erosion in the Alps (Lehmann et al., 2022; Müller et al., 2014, 2016) and Alaska (Wahrhaftig & Cox, 1959), for cirque glacier erosion in British Columbia (Sanders et al., 2013), and with compilations of rockwall erosion rates (Draebing et al., 2022) confirming that rock glaciers are an important part of the alpine debris-transport system (Degenhardt, 2009).

6. Conclusions

The RG-2 rock glacier in the Uinta Mountains of Utah is an active periglacial feature currently moving with a surface velocity of ~10 cm yr^{-1}. Cosmogenic surface-exposure ages of boulders conveyed downslope on the rock glacier surface indicate that RG-2 has been in existence since at least 10 ka, near the start of the Holocene. These ages, combined with the current dimensions of RG-2, correspond to a long-term surface velocity of ~3 ± 0.3 cm yr^{-1}. The discrepancy between modern and long-term surface velocities demonstrates that rock glacier movement can vary significantly over time. RG-2 does not appear to have an ice core, at least at its rooting zone where rock debris and ice are added through mass wasting and burial of snow. Over the course of the Holocene, RG-2 has transported a volume of rock debris equivalent to ~10 m of headward erosion of the cirque headwall above it. Our results demonstrate that rock glaciers can be long-lived dynamic components of periglacial systems capable of shaping landscapes, transporting sediment, and responding to climatic forcing over millennia.

Data Availability Statement

Copernicus Sentinel-1 data [2016–2021] were retrieved from the Alaska Satellite Facility Distributed Active Archive Center (Alaska Satellite Facility, 2024). SAR data were processed using MintPy, the Miami INsar Time-series software in Python (MintPy, 2014/2024) and ISCE, the Interferometric synthetic aperture radar Scientific Computing Environment (InSAR Scientific Computing Environment, 2019/2024). Climate data for the Chepeta SNOTEL site provided by the U.S. Department of Agriculture Natural Resources Conservation Service (National Water and Climate Center, 2024). Digital elevation data were obtained from SRTM, the Shuttle Radar Topography Mission (Earth Resources Observation and Science (EROS) Center | U.S. Geological Survey, 2024). Data generated in this research are available in the Zenodo repository (Munroe, 2023).

Acknowledgments

This work was supported by NSF HS-1935200 to PIs Munroe and Handwerger. The authors thank C. Kluetmeier, S. Lusk, A. Santis, and A. Takoudes for their assistance in the field. Part of this research was carried out at the Jet Propulsion Laboratory, California Institute of Technology, under a contract with the National Aeronautics and Space Administration (80NM0018D0004). Cosmogenic data in this publication were generated with the support of NSF-EAR 1735676; we thank J. Drebber for assistance with sample preparation. Fieldwork took place in the ancestral homelands of the Ute tribe.

References

Alaska Satellite Facility. (2024). Retrieved from https://asf.alaska.edu/about-asf-daac/

Amschwand, D., Ivy-Ochs, S., Frehner, M., Steinemann, O., Christl, M., & Vockenhuber, C. (2021). Deciphering the evolution of the Bleis Marscha rock glacier (Val d'Err, eastern Switzerland) with cosmogenic nuclide exposure dating, aerial image correlation, and finite element modeling. *The Cryosphere*, *15*(4), 2057–2081. https://doi.org/10.5194/tc-15-2057-2021

Anderson, R. S., Anderson, L. S., Armstrong, W. H., Rossi, M. W., & Crump, S. E. (2018). Glaciation of alpine valleys: The glacier–debris-covered glacier–rock glacier continuum. *Geomorphology*, *311*, 127–142. https://doi.org/10.1016/j.geomorph.2018.03.015

Arenson, L. U., Hoelzle, M., & Springman, S. (2002). Borehole deformation measurements and internal structure of some rock glaciers in Switzerland. *Permafrost and Periglacial Processes*, *13*(2), 117–135. https://doi.org/10.1002/ppp.414

Arenson, L. U., & Jakob, M. (2010). The significance of rock glaciers in the dry Andes–a discussion of Azócar and Brenning (2010) and Brenning and Azócar (2010). *Permafrost and Periglacial Processes*, *21*(3), 282–285. https://doi.org/10.1002/ppp.693

Balco, G. (2008). CRONUS-Earth online calculators.

Baroni, C., Carton, A., & Seppi, R. (2004). Distribution and behaviour of rock glaciers in the Adamello–Presanella Massif (Italian Alps). *Permafrost and Periglacial Processes*, *15*(3), 243–259. https://doi.org/10.1002/ppp.497

Barsch, D. (1987). The problem of the ice-cored rock glacier. *Rock Glaciers*, 45–53.

Berthling, I. (2011). Beyond confusion: Rock glaciers as cryo-conditioned landforms. *Geomorphology*, *131*(3–4), 98–106. https://doi.org/10.1016/j.geomorph.2011.05.002

Bertone, A., Seppi, R., Callegari, M., Cuozzo, G., Dematteis, N., Krainer, K., et al. (2023). Unprecedented observation of hourly rock glacier velocity with ground-based SAR. *Geophysical Research Letters*, *50*(9), e2023GL102796. https://doi.org/10.1029/2023gl102796

Borchers, B., Marrero, S., Balco, G., Caffee, M., Goehring, B., Lifton, N., et al. (2016). Geological calibration of spallation production rates in the CRONUS-Earth project. *Quaternary Geochronology*, *31*, 188–198. https://doi.org/10.1016/j.quageo.2015.01.009

Bradley, M. D. (1995). Timing of the Laramide rise of the Uinta Mountains, Utah and Colorado. In *Guidebook - Wyoming geological association, 1995* (pp. 31–44).

Brencher, G., Handwerger, A. L., & Munroe, J. S. (2021). InSAR-based characterization of rock glacier movement in the Uinta Mountains, Utah, USA. *The Cryosphere*, *15*(10), 4823–4844. https://doi.org/10.5194/tc-15-4823-2021

Brighenti, S., Hotaling, S., Finn, D. S., Fountain, A. G., Hayashi, M., Herbst, D., et al. (2021). Rock glaciers and related cold rocky landforms: Overlooked climate refugia for mountain biodiversity. *Global Change Biology*, *27*(8), 1504–1517. https://doi.org/10.1111/gcb.15510

Charton, J., Verfaillie, D., Jomelli, V., Francou, B., & Team, A. (2021). Early Holocene rock glacier stabilisation at col du Lautaret (French Alps): Palaeoclimatic implications. *Geomorphology*, *394*, 107962. https://doi.org/10.1016/j.geomorph.2021.107962

Cicoira, A., Beutel, J., Faillettaz, J., Gärtner-Roer, I., & Vieli, A. (2019). Resolving the influence of temperature forcing through heat conduction on rock glacier dynamics: A numerical modelling approach. *The Cryosphere*, *13*(3), 927–942. https://doi.org/10.5194/tc-13-927-2019

Çiner, A., Sarıkaya, M. A., & Yıldırım, C. (2017). Misleading old age on a young landform? The dilemma of cosmogenic inheritance in surface exposure dating: Moraines vs. rock glaciers. *Quaternary Geochronology*, *42*, 76–88. https://doi.org/10.1016/j.quageo.2017.07.003

Corbett, L. B., Bierman, P. R., & Rood, D. H. (2016). An approach for optimizing in situ cosmogenic 10Be sample preparation. *Quaternary Geochronology*, *33*, 24–34. https://doi.org/10.1016/j.quageo.2016.02.001

Corbett, L. B., Bierman, P. R., Woodruff, T. E., & Caffee, M. W. (2019). A homogeneous liquid reference material for monitoring the quality and reproducibility of in situ cosmogenic 10Be and 26Al analyses. *Nuclear Instruments and Methods in Physics Research Section B: Beam Interactions with Materials and Atoms*, *456*, 180–185. https://doi.org/10.1016/j.nimb.2019.05.051

Degenhardt, J. J. (2009). Development of tongue-shaped and multilobate rock glaciers in alpine environments – Interpretations from ground penetrating radar surveys. *Geomorphology*, *109*(3), 94–107. https://doi.org/10.1016/j.geomorph.2009.02.020

Degenhardt, J. J., & Giardino, J. R. (2003). Subsurface investigation of a rock glacier using ground-penetrating radar: Implications for locating stored water on Mars. *Journal of Geophysical Research*, *108*(E4), 8036. https://doi.org/10.1029/2002je001888

Degenhardt, J. J., Giardino, J. R., & Junck, M. B. (2003). GPR survey of a lobate rock glacier in Yankee Boy Basin, Colorado, USA. *Geological Society, London, Special Publications*, *211*(1), 167–179. https://doi.org/10.1144/gsl.sp.2001.211.01.14

Draebing, D., Mayer, T., Jacobs, B., & McColl, S. T. (2022). Alpine rockwall erosion patterns follow elevation-dependent climate trajectories. *Communications Earth & Environment*, *3*(1), 1–12. https://doi.org/10.1038/s43247-022-00348-2

Earth Resources Observation and Science (EROS) Center, U.S. Geological Survey. (2024). Retrieved from https://www.usgs.gov/centers/eros

Farr, T. G., Rosen, P. A., Caro, E., Crippen, R., Duren, R., Hensley, S., et al. (2007). The shuttle radar topography mission. *Reviews of Geophysics*, *45*(2). https://doi.org/10.1029/2005RG000183

Fattahi, H., & Amelung, F. (2013). DEM error correction in InSAR time series. *IEEE Transactions on Geoscience and Remote Sensing*, *51*(7), 4249–4259. https://doi.org/10.1109/tgrs.2012.2227761

Florentine, C., Skidmore, M., Speece, M., Link, C., & Shaw, C. A. (2014). Geophysical analysis of transverse ridges and internal structure at Lone Peak Rock Glacier, Big Sky, Montana, USA. *Journal of Glaciology*, *60*(221), 453–462. https://doi.org/10.3189/2014JoG13J160

Frehner, M., Ling, A. H. M., & Gärtner-Roer, I. (2015). Furrow-and-ridge morphology on rockglaciers explained by gravity-driven buckle folding: A case study from the Murtèl Rockglacier (Switzerland). *Permafrost and Periglacial Processes*, *26*(1), 57–66. https://doi.org/10.1002/ppp.1831

Giardino, J. R., Shroder, J. F., & Vitek, J. D. (1987). *Rock glaciers*. Allen & Unwin.

Giardino, J. R., & Vitek, J. D. (1988). The significance of rock glaciers in the glacial-periglacial landscape continuum. *Journal of Quaternary Science*, *3*(1), 97–103. https://doi.org/10.1002/jqs.3390030111

Gosse, J. C., & Phillips, F. M. (2001). Terrestrial in situ cosmogenic nuclides: Theory and application. *Quaternary Science Reviews*, *20*(14), 1475–1560. https://doi.org/10.1016/S0277-3791(00)00171-2

Green, M. D., Tronstad, L. M., Giersch, J. J., Shah, A. A., Fallon, C. E., Blevins, E., et al. (2022). Stoneflies in the genus Lednia (Plecoptera: Nemouridae): Sentinels of climate change impacts on mountain stream biodiversity. *Biodiversity & Conservation*, *31*(2), 353–377. https://doi.org/10.1007/s10531-021-02344-y

Haeberli, W. (1985). Creep of mountain permafrost: Internal structure and flow of alpine rock glaciers. *Mitteilungen Der Versuchsanstalt Fur Wasserbau, Hydrologie Und Glaziologie an Der Eidgenossischen Technischen Hochschule Zurich*(77).

Hotaling, S., Hood, E., & Hamilton, T. L. (2017). Microbial ecology of mountain glacier ecosystems: Biodiversity, ecological connections and implications of a warming climate. *Environmental Microbiology*, *19*(8), 2935–2948. https://doi.org/10.1111/1462-2920.13766

Hotaling, S., Shah, A. A., McGowan, K. L., Tronstad, L. M., Giersch, J. J., Finn, D. S., et al. (2020). Mountain stoneflies may tolerate warming streams: Evidence from organismal physiology and gene expression. *Global Change Biology*, *26*(10), 5524–5538. https://doi.org/10.1111/gcb.15294

Ikeda, A., Matsuoka, N., & Kääb, A. (2008). Fast deformation of perennially frozen debris in a warm rock glacier in the Swiss Alps: An effect of liquid water. *Journal of Geophysical Research*, *113*(F1). https://doi.org/10.1029/2007jf000859

InSAR Scientific Computing Environment. (2024). (Version 2). isce-framework. Retrieved from https://github.com/isce-framework/isce2

Janke, J. R. (2007). Colorado front range rock glaciers: Distribution and topographic characteristics. In *1, Special section: Proceedings of the fifth circumpolar ecosystems conference and workshop, Churchill, Manitoba, Canada, February 2004*. In *Arctic, Antarctic, and alpine research* (Vol. 39, pp. 74–83).

Janke, J. R., Ng, S., & Bellisario, A. (2017). An inventory and estimate of water stored in firn fields, glaciers, debris-covered glaciers, and rock glaciers in the Aconcagua River Basin, Chile. *Geomorphology*, *296*, 142–152. https://doi.org/10.1016/j.geomorph.2017.09.002

Janke, J. R., Regmi, N. R., Giardino, J. R., & Vitek, J. D. (2013). Rock glaciers. In J. F. Shroder (Ed.), *Treatise on geomorphology* (pp. 238–273). Academic Press. https://doi.org/10.1016/B978-0-12-374739-6.00211-6

Jolivet, R., Grandin, R., Lasserre, C., Doin, M.-P., & Peltzer, G. (2011). Systematic InSAR tropospheric phase delay corrections from global meteorological reanalysis data. *Geophysical Research Letters*, *38*(17), L17311. https://doi.org/10.1029/2011gl048757

Jones, D. B., Harrison, S., Anderson, K., & Whalley, W. B. (2019). Rock glaciers and mountain hydrology: A review. *Earth-Science Reviews*, *193*, 66–90. https://doi.org/10.1016/j.earscirev.2019.04.001

Kääb, A., Frauenfelder, R., & Roer, I. (2007). On the response of rockglacier creep to surface temperature increase. *Global and Planetary Change*, *56*(1), 172–187. https://doi.org/10.1016/j.gloplacha.2006.07.005

Kääb, A., & Reichmuth, T. (2005). Advance mechanisms of rock glaciers. *Permafrost and Periglacial Processes*, *16*(2), 187–193. https://doi.org/10.1002/ppp.507

Kääb, A., & Weber, M. (2004). Development of transverse ridges on rock glaciers: Field measurements and laboratory experiments. *Permafrost and Periglacial Processes*, *15*(4), 379–391. https://doi.org/10.1002/ppp.506

Kenner, R., Bühler, Y., Delaloye, R., Ginzler, C., & Phillips, M. (2014). Monitoring of high alpine mass movements combining laser scanning with digital airborne photogrammetry. *Geomorphology*, *206*, 492–504. https://doi.org/10.1016/j.geomorph.2013.10.020

Kenner, R., Phillips, M., Beutel, J., Hiller, M., Limpach, P., Pointner, E., & Volken, M. (2017). Factors controlling velocity variations at short-term, seasonal and multiyear time scales, Ritigraben rock glacier, Western Swiss Alps. *Permafrost and Periglacial Processes*, *28*(4), 675–684. https://doi.org/10.1002/ppp.1953

Kenner, R., Pruessner, L., Beutel, J., Limpach, P., & Phillips, M. (2020). How rock glacier hydrology, deformation velocities and ground temperatures interact: Examples from the Swiss Alps. *Permafrost and Periglacial Processes*, *31*(1), 3–14. https://doi.org/10.1002/ppp.2023

Knight, J., Harrison, S., & Jones, D. B. (2019). Rock glaciers and the geomorphological evolution of deglacierizing mountains. *Geomorphology*, *324*, 14–24. https://doi.org/10.1016/j.geomorph.2018.09.020

Kohl, C. P., & Nishiizumi, K. (1992). Chemical isolation of quartz for measurement of in-situ -produced cosmogenic nuclides. *Geochimica et Cosmochimica Acta*, *56*(9), 3583–3587. https://doi.org/10.1016/0016-7037(92)90401-4

Konrad, S. K., Humphrey, N. F., Steig, E. J., Clark, D. H., Potter, N., & Pfeffer, W. T. (1999). Rock glacier dynamics and paleoclimatic implications. *Geology*, *27*(12), 1131–1134. https://doi.org/10.1130/0091-7613(1999)027<1131:rgdapi>2.3.co;2

Krainer, K., Bressan, D., Dietre, B., Haas, J. N., Hajdas, I., Lang, K., et al. (2015). A 10,300-year-old permafrost core from the active rock glacier Lazaun, southern Ötztal Alps (South Tyrol, northern Italy). *Quaternary Research*, *83*(02), 324–335. https://doi.org/10.1016/j.yqres.2014.12.005

Krainer, K., & He, X. (2006). Flow velocities of active rock glaciers in the Austrian Alps. *Geografiska Annaler - Series A: Physical Geography*, *88*(4), 267–280. https://doi.org/10.1111/j.0435-3676.2006.00300.x

Lambiel, C., & Delaloye, R. (2004). Contribution of real-time kinematic GPS in the study of creeping mountain permafrost: Examples from the Western Swiss Alps. *Permafrost and Periglacial Processes*, *15*(3), 229–241. https://doi.org/10.1002/ppp.496

Lehmann, B., Anderson, R. S., Bodin, X., Cusicanqui, D., Valla, P. G., & Carcaillet, J. (2022). Alpine rock glacier activity over Holocene to modern timescales (western French Alps). *Earth Surface Dynamics Discussions*, *10*(3), 1–40. https://doi.org/10.5194/esurf-10-605-2022

Lifton, N., Caffee, M., Finkel, R., Marrero, S., Nishiizumi, K., Phillips, F. M., et al. (2015). In situ cosmogenic nuclide production rate calibration for the CRONUS-Earth project from Lake Bonneville, Utah, shoreline features. *Quaternary Geochronology*, *26*, 56–69. https://doi.org/10.1016/j.quageo.2014.11.002

Lifton, N., Sato, T., & Dunai, T. J. (2014). Scaling in situ cosmogenic nuclide production rates using analytical approximations to atmospheric cosmic-ray fluxes. *Earth and Planetary Science Letters*, *386*, 149–160. https://doi.org/10.1016/j.epsl.2013.10.052

Liu, L., Millar, C. I., Westfall, R. D., & Zebker, H. A. (2013). Surface motion of active rock glaciers in the Sierra Nevada, California, USA: Inventory and a case study using InSAR. *The Cryosphere*, *7*(4), 1109–1119. https://doi.org/10.5194/tc-7-1109-2013

Marcer, M., Cicoira, A., Cusicanqui, D., Bodin, X., Echelard, T., Obregon, R., & Schoeneich, P. (2021). Rock glaciers throughout the French Alps accelerated and destabilised since 1990 as air temperatures increased. *Communications Earth & Environment*, *2*(1), 81. https://doi.org/10.1038/s43247-021-00150-6

Merz, K., Maurer, H., Buchli, T., Horstmeyer, H., Green, A. G., & Springman, S. M. (2015). Evaluation of ground-based and helicopter ground-penetrating radar data acquired across an alpine rock glacier. *Permafrost and Periglacial Processes*, *26*(1), 13–27. https://doi.org/10.1002/ppp.1836

Millar, C. I., & Westfall, R. D. (2008). Rock glaciers and related periglacial landforms in the Sierra Nevada, CA, USA; inventory, distribution and climatic relationships. *Quaternary International*, *188*(1), 90–104. https://doi.org/10.1016/j.quaint.2007.06.004

MintPy. (2024). Python, insarlab. Retrieved from https://github.com/insarlab/MintPy

Monnier, S., & Kinnard, C. (2013). Internal structure and composition of a rock glacier in the Andes (upper Choapa valley, Chile) using borehole information and ground-penetrating radar. *Annals of Glaciology*, *54*(64), 61–72. https://doi.org/10.3189/2013aog64a107

Moran, A. P., Ivy Ochs, S., Vockenhuber, C., & Kerschner, H. (2016). Rock glacier development in the Northern Calcareous Alps at the Pleistocene-Holocene boundary. *Geomorphology*, *273*, 178–188. https://doi.org/10.1016/j.geomorph.2016.08.017

Mühll, D. S. V., & Holub, P. (1992). Borehole logging in alpine permafrost, upper Engadin, Swiss Alps. *Permafrost and Periglacial Processes*, *3*(2), 125–132. https://doi.org/10.1002/ppp.3430030209

Müller, J., Gärtner-Roer, I., Kenner, R., Thee, P., & Morche, D. (2014). Sediment storage and transfer on a periglacial mountain slope (Corvatsch, Switzerland). *Geomorphology*, *218*, 35–44. https://doi.org/10.1016/j.geomorph.2013.12.002

Müller, J., Vieli, A., & Gärtner-Roer, I. (2016). Rock glaciers on the run - Understanding rock glacier landform evolution and recent changes from numerical flow modeling. *The Cryosphere*, *10*(6), 2865–2886. https://doi.org/10.5194/tc-10-2865-2016

Munroe, J. S. (2002). Timing of postglacial cirque reoccupation in the northern Uinta Mountains, northeastern Utah, USA. *Arctic Antarctic and Alpine Research*, *34*, 38–48. https://doi.org/10.2307/1552507

Munroe, J. S. (2003). Estimates of Little ice age climate inferred through historical rephotography, northern Uinta Mountains, USA. *Arctic Antarctic and Alpine Research*, *35*(4), 489–498. https://doi.org/10.1657/1523-0430(2003)035[0489:eoliac]2.0.co;2

Munroe, J. S. (2018). Distribution, evidence for internal ice, and possible hydrologic significance of rock glaciers in the Uinta Mountains, Utah, USA. *Quaternary Research*, *90*(1), 1–16. https://doi.org/10.1017/qua.2018.24

Munroe, J. S. (2023). Datafiles resulting from work at the RG-2 rock glacier in the Uinta Mountains, 2021-2022 [Dataset]. *Zenodo*. https://doi.org/10.5281/zenodo.8367559

Munroe, J. S., & Handwerger, A. L. (2023a). Contribution of rock glacier discharge to late summer and fall streamflow in the Uinta Mountains, Utah, USA. *Hydrology and Earth System Sciences*, *27*(2), 543–557. https://doi.org/10.5194/hess-27-543-2023

Munroe, J. S., & Handwerger, A. L. (2023b). Examining the variability of rock glacier meltwater in space and time in high-elevation environments of Utah, United States. *Frontiers in Earth Science*, *11*, 1129314. https://doi.org/10.3389/feart.2023.1129314

Munroe, J. S., Klem, C. M., & Bigl, M. F. (2013). A lacustrine sedimentary record of Holocene periglacial activity from the Uinta Mountains, Utah, U.S.A. *Quaternary Research*, *79*(2), 101–109. https://doi.org/10.1016/j.yqres.2012.12.006

Munroe, J. S., & Laabs, B. J. (2017). Combining radiocarbon and cosmogenic ages to constrain the timing of the last glacial-interglacial transition in the Uinta Mountains, Utah, USA. *Geology*, *45*(2), 171–174. https://doi.org/10.1130/g38156.1

Munroe, J. S., & Laabs, B. J. C. (2009). Glacial geologic map of the Uinta Mountains Area, Utah and Wyoming.

Naftz, D. L., Klusman, R. W., Michel, R. L., Schuster, P. F., Reddy, M. M., Taylor, H. E., et al. (1996). Little Ice Age evidence from a south-central North American ice core, USA. *Arctic and Alpine Research*, *28*(1), 35–41. https://doi.org/10.2307/1552083

National Water and Climate Center. (2024). Chepeta SNOTEL (396). Retrieved from https://wcc.sc.egov.usda.gov/nwcc/site?sitenum=396

Nickus, U., Abermann, J., Fischer, A., Krainer, K., Schneider, H., Span, N., & Thies, H. (2015). Rock Glacier Äußeres Hochebenkar (Austria)–recent results of a monitoring network. *Zeitschrift für Gletscherkunde und Glazialgeologie*, *47*(48), 43–62.

Nishiizumi, K., Imamura, M., Caffee, M. W., Southon, J. R., Finkel, R. C., & McAninch, J. (2007). Absolute calibration of ^{10}Be AMS standards. *Nuclear Instruments and Methods in Physics Research Section B: Beam Interactions with Materials and Atoms*, *258*(2), 403–413. https://doi.org/10.1016/j.nimb.2007.01.297

Obu, J., Westermann, S., Bartsch, A., Berdnikov, N., Christiansen, H. H., Dashtseren, A., et al. (2019). Northern Hemisphere permafrost map based on TTOP modelling for 2000–2016 at 1 km^2 scale. *Earth-Science Reviews*, *193*, 299–316. https://doi.org/10.1016/j.earscirev.2019.04.023

Petersen, E. I., Levy, J. S., Holt, J. W., & Stuurman, C. M. (2020). New insights into ice accumulation at Galena Creek Rock Glacier from radar imaging of its internal structure. *Journal of Glaciology*, *66*(255), 1–10. https://doi.org/10.1017/jog.2019.67

Potter, N. (1972). Ice-cored rock glacier, Galena Creek, northern Absaroka Mountains, Wyoming. *Geological Society of America Bulletin*, *83*(10), 3025–3058. https://doi.org/10.1130/0016-7606(1972)83[3025:irggcn]2.0.co;2

Rangecroft, S., Harrison, S., & Anderson, K. (2015). Rock glaciers as water stores in the Bolivian Andes: An assessment of their hydrological importance. *Arctic Antarctic and Alpine Research*, *47*(1), 89–98. https://doi.org/10.1657/AAAR0014-029

Reynolds, J. M. (2011). *An introduction to applied and environmental geophysics*. John Wiley & Sons.

Rode, M., & Kellerer-Pirklbauer, A. (2012). Schmidt-hammer exposure-age dating (SHD) of rock glaciers in the Schöderkogel-Eisenhut area, Schladminger Tauern Range, Austria. *The Holocene*, *22*(7), 761–771. https://doi.org/10.1177/0959683611430410

Rosen, P. A., Gurrola, E., Sacco, G. F., & Zebker, H. (2012). The InSAR scientific computing environment. In *EUSAR 2012; 9th European conference on synthetic aperture radar* (pp. 730–733). VDE.

Sadler, P. M. (1981). Sediment accumulation rates and the completeness of stratigraphic sections. *The Journal of Geology*, *89*(5), 569–584. https://doi.org/10.1086/628623

Sanders, J. W., Cuffey, K. M., MacGregor, K. R., & Collins, B. D. (2013). The sediment budget of an alpine cirque. *Bulletin*, *125*(1–2), 229–248. https://doi.org/10.1130/b30688.1

Scapozza, C., Lambiel, C., Bozzini, C., Mari, S., & Conedera, M. (2014). Assessing the rock glacier kinematics on three different timescales: A case study from the southern Swiss Alps. *Earth Surface Processes and Landforms*, *39*(15), 2056–2069. https://doi.org/10.1002/esp.3599

Wagner, T., Kainz, S., Helfricht, K., Fischer, A., Avian, M., Krainer, K., & Winkler, G. (2021). Assessment of liquid and solid water storage in rock glaciers versus glacier ice in the Austrian Alps. *Science of the Total Environment*, *800*, 149593. https://doi.org/10.1016/j.scitotenv.2021.149593

Wahrhaftig, C., & Cox, A. (1959). Rock glaciers in the Alaska Range. *Geological Society of America Bulletin*, *70*(4), 383–436. https://doi.org/10.1130/0016-7606(1959)70[383:rgitar]2.0.co;2

Wayne, W. J. (1981). Ice segregation as an origin for lenses of non-glacial ice in "ice-cemented" rock glaciers. *Journal of Glaciology*, *27*(97), 506–510. https://doi.org/10.3189/s0022143000011564

Winkler, G., Wagner, T., Pauritsch, M., Birk, S., Kellerer-Pirklbauer, A., Benischke, R., et al. (2016). Identification and assessment of groundwater flow and storage components of the relict Schöneben Rock Glacier, Niedere Tauern Range, Eastern Alps (Austria). *Hydrogeology Journal*, *24*(4), 937–953. https://doi.org/10.1007/s10040-015-1348-9

Wirz, V., Gruber, S., Purves, R. S., Beutel, J., Gärtner-Roer, I., Gubler, S., & Vieli, A. (2016). Short-term velocity variations at three rock glaciers and their relationship with meteorological conditions. *Earth Surface Dynamics*, *4*(1), 103–123. https://doi.org/10.5194/esurf-4-103-2016

Yunjun, Z., Fattahi, H., & Amelung, F. (2019). Small baseline InSAR time series analysis: Unwrapping error correction and noise reduction. *Computers & Geosciences*, *133*, 104331. https://doi.org/10.1016/j.cageo.2019.104331